CHEMISTRY OF MATERIALS

COMMUNICATION

pubs.acs.org/cm

Three-Dimensional Spatial Distribution of Cr atoms in Doped Indium Oxide

David J. Payne*,† and Emmanuelle A. Marquis‡,§

†Department of Chemistry, Chemistry Research Laboratory, University of Oxford, 12 Mansfield Road, Oxford, OX1 3TA, United Kingdom

‡ Department of Materials, University of Oxford, Parks Road, Oxford OX1 3PH, United Kingdom

KEYWORDS: characterization of materials, atom-probe tomography, dilute magnetic oxides

Since the first experimental confirmation of room temperature ferromagnetism by Matsumoto et al. in 2001, upon doping Co into TiO_2,[1] the field of dilute magnetic oxides (DMOs) has grown exponentially. Since then, there have been claims of dilute semiconductor ferromagnetism in a wide range of doped oxides systems including TiO_2 doped with V, Co, and Fe, ZnO doped with V, Mn, Fe, Cu, Co, and Ni, and SnO_2 doped with Fe and Co.[2]

Understanding how magnetism arises within these systems has long been a source of contention. Due to the considerably lower doping levels (<5%) found within "dilute" magnetic oxides, conventional models of magnetism (i.e. super exchange or double exchange models, which rely on doping levels >10%)) cannot explain the observed phenomenon. As a result, numerous theoretical models have been developed in an attempt to understand and clarify the phenomenon, detailed descriptions of which can be found in a number of thorough review articles.[3−6]

In 2006, Cr-doped In_2O_3 was reported as a possible DMO candidate material.[7] Thin fims were found to undergo a transition from an insulating paramagnetic state to a ferromagnetic semiconducting state with increasing defect concentration, with a T_c of 850−930 K. This generated a flurry of interest,[8−11] due, in part, to the fact that In_2O_3 is the prototypical transparent conducting oxide (TCO) material. Combining ferromagnetic behavior with high optical transparency and conductivity, offers a tantalising opportunity for spin-electronic applications.[12] Unfortunately, initial optimism soon turned to scepticism, as the material was shown to not display room-temperature ferromagnetic behavior in bulk, ceramic samples.[13] It therefore remains a significant challenge to understand the unique magnetic phenomenon, which occurs in this and many other systems.

Attempts to determine the origin of this behavior have led to some interesting arguments. Raebiger et al.[14] use density functional theory (DFT) within a band gap corrected approach to suggest that ferromagnetism can be turned on and off via extrinsic n-type doping (substitutional Sn) and that these additional carriers stabilize the ferromagnetic Cr coupling. Recent experimental work has demonstrated that the band gap of In_2O_3 is less than 3 eV,[15,16] meaning that the further theoretical work concerning the placement of chromium levels within the host conduction band needs to be carefully considered. It has also been argued that p-type intrinsic defects such as In vacancies or O interstitials mediate ferromagnetism.[17] It is clear that there remains uncertainty over the source of ferromagnetism in Cr-doped In_2O_3, because of the lack of control over growth conditions and knowledge of structure and chemistry of the films.

To date, there remain significant experimental challenges associated with characterizing these materials. Sample contamination from the use of stainless steel tweezers is one of them. It has been noted that just 20 ng of contaminant, in a thin film sample, is enough to give rise to intrinsic DMO behavior.[2] While it is possible to remove the risk of contamination, determining dopant inhomogeneity, clustering, or presence of secondary phases (for example, CrO_2 is a metallic ferromagnet) remains a significant technological issue. Techniques such as X-ray diffraction (XRD), high-resolution transmission electron microscopy (HRTEM), secondary ion mass spectrometry (SIMS), and Rutherford Backscattering are often utilized to characterize the structure of DMO systems[18] yet lack the required chemical sensitivity and/or spatial resolution to detect clustering on the atomic scale. While aberration corrected analytical techniques such as high resolution EELS might in theory be able to detect small clusters, the analyses remain limited to a 2D projection.

Atom-probe tomography (APT) is a 3D imaging technique combining field evaporation from specimen in the form of sharp needles with apex radii of curvature < 100 nm, time-of-flight mass spectrometry, and position sensitive detection. It has typically been the technique of choice for investigating clustering in metallic systems.[19] With the development of fast and stable laser systems, semiconductor and oxide materials can be quantitatively analyzed at the nanometer scale.[20,21] Recently, APT was used by Larde et al.[22] to investigate Co-doped ZnO, where no Co clustering, or patterning, was observed. The current study is concerned with Cr-doped In_2O_3, where a clear inhomogeneity in the film is observed, yet no ferromagnetism is present.

Synthesis of ceramic pellets of 6.25% Cr-doped In_2O_3 were prepared by the solid state reaction of the appropriate ratios of In_2O_3 (Sigma-Aldrich, 99.99%) and Cr_2O_3 (Sigma-Aldrich, 99.9%). The pellets were fired in a muffle furnace in recrystallized alumina boats at 1400 °C for 48 h. Thin films were synthesized via electron beam evaporation (Varian, model 3120). Oxygen was let into the chamber to a pressure of 1.6×10^{-5} mbar. The pressure during coating was 1.8×10^{-5} mbar. An electron beam was directed to the (as prepared 6.25% Cr-doped In_2O_3) ceramic

Received: December 1, 2010
Revised: January 26, 2011
Published: February 11, 2011

dx.doi.org/10.1021/cm103439e | *Chem. Mater.* 2011, 23, 1085–1087

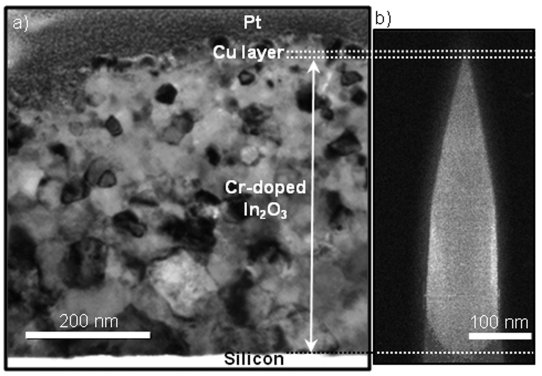

Figure 1. (a) Bright field TEM image of a cross section specimen. (b) Scanning electron image of an atom probe specimen (to scale).

sample, with an evaporation rate of between 1 and 4 nm/s, which resulted in a polycrystalline film of approximately 500 nm thickness grown on Si(100) substrates (10 mm^2 × 0.5 mm). The film was then postannealed in air at 600 °C. X-ray diffraction experiments were performed using a Phillips Xpert powder diffractometer (operating in a $\Theta-2\Theta$ configuration), confirming the phase purity and the polycrystalline nature of the ceramic and thin film samples. No evidence of secondary phases was detected with the preferred orientation in the (222) plane. Meticulous care was taken to ensure that no ferromagnetic materials could contaminate the sample. Magnetic measurements on bulk, ceramic samples were obtained on a Quantum Design MPMS (Magnetic Property Measurement System) XL SQUID magnetometer. Thin-film magnetic measurements were performed on a temperature controlled ADE model 10 Mark II vibrating sample magnetometer. The bulk, ceramic material showed paramagnetic behavior and displayed no evidence of ferromagnetism, from 5 K to room temperature, and the thin film sample also displayed no evidence of ferromagnetism. A 50 nm thick sacrificial copper layer was deposited on top of the film to facilitate the atom-probe specimen preparation and limit damage due to the Ga beam. Atom-probe specimens were prepared by standard lift-out methods[23] using a Zeiss NVision dual beam focused ion beam instrument equipped with a Kleindiek micromanipulator. Specimens were mounted on Si needles, and final sharpening was performed using 2 kV Ga^+ beam. Atom probe analyses were performed using a Cameca LEAP 3000HR microscope operated in laser pulsing mode (532 nm wavelength, 3 ns pulse length). Note that while the use of a shorter wavelength might have improved the mass resolution,[24] the spatial resolution remains unaffected by the laser conditions that were chosen to ensure mininal specimen heating. Specimens were cooled to 50 K, and are pulses were applied with a repetition rate of 200 kHz, pulse energy between 0.2 and 0.3 nJ, and a 10 μm (4 σ) spot size. TEM specimens were prepared by a standard lift-out method using either a Zeiss NVision or a FEI Helios instrument. TEM observations were performed on a Philips CM20 microscope operated at 200 kV.

The films exhibit fine grain size as measured by XRD and (the Scherrer equation was used, giving an average of 39 ± 4 nm) and TEM observations of cross section specimens. A representative TEM image in Figure 1 shows the fine grain structure of the film with somewhat larger grain sizes near the substrate. The geometry of an atom-probe specimen is shown in Figure 1b. A typical mass spectrum is shown in Figure 2. Indium evaporates as atomic species (In^+, In^{2+}, In^{3+}) and no charged molecular In_x species

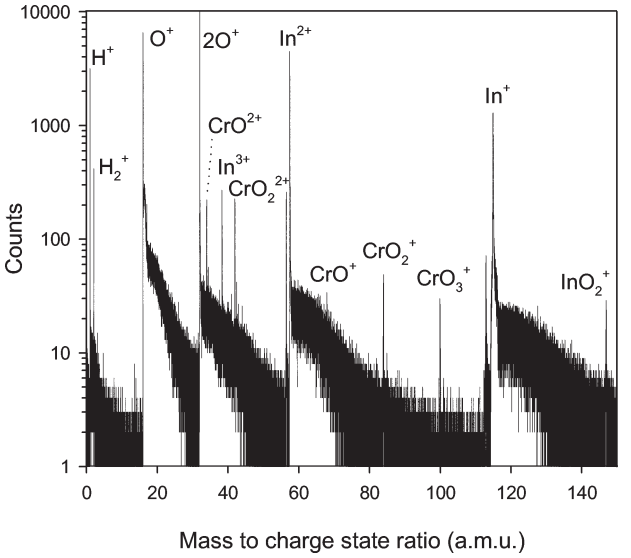

Figure 2. Representative mass spectrum.

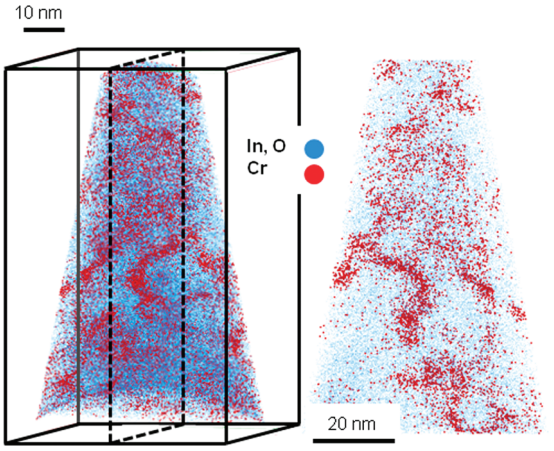

Figure 3. (a) 3D reconstruction of In, O, and Cr distribution throughout the tip, including a cross sectional 5 nm thick slide shown in (b).

are observed (with the exception of InO_2^+). Oxygen is evaporated as both atomic and molecular species (O, O_2). Chromium on the other hand is mainly observed associated with oxygen (CrO^+, CrO_2^+, CrO_3^+). The overall measured composition is very close to the expected stochiometric composition (In_2O_3), 63.3 ± 1.1 atom % O, 35.5 ± 1.7 atom % In, with 1.2 ± 0.5 atom % Cr. The measured Cr content is lower than the nominal composition possibly due to loss during deposition. Another possible source of error originates from the limited detection efficiency of delay line detectors with respect to events close in time and space. In the case of In_2O_3 in particular, the number of detector events involving more than one hit per pulse is of the order of 45%. This number could not be decreased by changing the evaporation conditions. Although the distribution of multiple events appears to affect all elements equally, preferential loss of Cr is possible.

As illustrated in Figure 3, the Cr spatial distribution is inhomogeneous and the topology of the Cr distribution suggests that Cr forms clusters and may be preferentially located at grain boundaries and at triple lines. The spacing between the Cr-rich regions is indeed consistent with the grain sizes observed by electron microscopy (Figure 1) and those measured by X-ray

dx.doi.org/10.1021/cm103439e |*Chem. Mater.* 2011, 23, 1085–1087

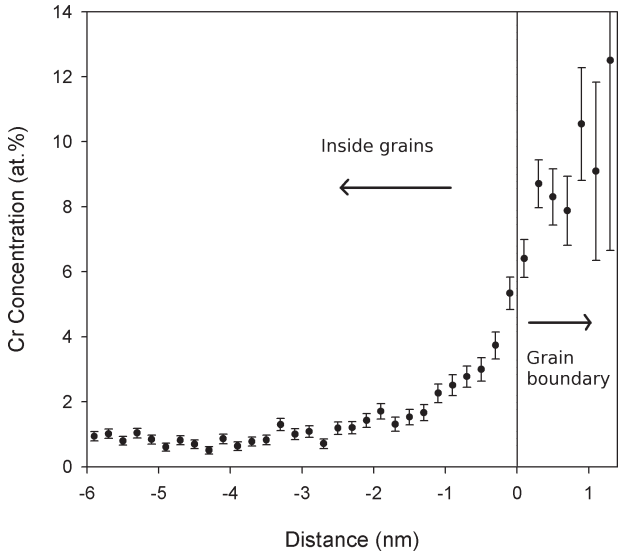

Figure 4. Proximity histogram based on a 3% Cr iso-surface.

diffraction (39 ± 4.0 nm). To reveal the average Cr concentration at the grain boundaries, a proximity histogram[25] (Figure 4) based on a 3 atom % Cr iso-surface is constructed. The Cr concentration reaches above 8 atom % at the grain boundaries and drops to 1 atom % inside the grains. The bulk solubility limit of Cr in In_2O_3 is 7.5%.[26] The segregation of Cr at grain boundaries and presumably the film surface may result from the specific growth conditions and annealing treatment, while the grain structure will be strongly influenced by the choice of substrate.

In conclusion, within the theoretical framework of DMO materials, the absence of magnetism can be related to Cr segregation to grain boundaries and consequently to a low level of Cr incorporated in the matrix. The presence of clustering demonstrates that clustering alone is also *not* a source magnetism for this material system. Further work is needed to determine, for example, the oxidation state of the chromium in the matrix, as well as the growth parameters such as oxygen partial pressure and annealing treatments on solute distribution.

Atomic scale chemical and structural characterization is a necessary path forward to visualize and understand the physical properties displayed by doped oxide systems. It is hoped that such a systematic approach will be applied to elucidate the DMO behavior as well as the properties of transparent conducting oxides (TCOs), particularly Sn-doped In_2O_3 (the ubiquitous indium tin oxide (ITO)).[27,28]

AUTHOR INFORMATION

Present Addresses

[§]Department of Materials Science and Engineering, University of Michigan, Ann Arbor, Michigan 48109-2136, USA.

ACKNOWLEDGMENT

This work was supported by the UK Royal Society (Research Grant RG080399 for D.J.P. and a Dorothy Hodgkin Fellowship for E.A.M.) and the UK Engineering and Physical Sciences Research Council. The authors thank Stephan Kraemer (UC Santa Barbara) for help with preparation of a TEM specimen and R.G. Egdell for stimulating dicussions. D.J.P. would like to thank Christ Church, University of Oxford, for the award of a Junior Research Fellowship.

REFERENCES

(1) Matsumoto, Y.; Murakami, M.; Shono, T.; Hasegawa, T.; Fukumura, T.; Kawasaki, M.; Ahmet, P.; Chikyow, T.; Koshihara, S.; Koinuma, H. *Science* **2001**, *291* (5505), 854–856.
(2) Coey, J. M. D. *Curr. Opin. Solid State Mater. Sci.* **2006**, *10*, 83–92.
(3) Jungwirth, T.; Sinova, J.; Mašek, J.; Kučera, J.; MacDonald, A. H. *Rev. Mod. Phys.* **2006**, *78*, 809–864.
(4) Pearton, S. J.; Heo, W. H.; Ivill, M.; Norton, D. P.; Steiner, T. *Semicond. Sci. Technol.* **2004**, *19*, R59–R74.
(5) Sato, K.; Bergqvist, L.; Kudrnovský, J.; Denderichs, P. H.; Eriksson, O.; Turek, I.; Sanyal, B.; Bouzerar, G.; Katayama-Yoshida, H.; Dinh, V. A.; Fukushima, T.; Kizaki, H.; Zeller, R. *Rev. Mod. Phys.* **2010**, *82*, 1633–1690.
(6) Dietl, T. *Nat. Mater.* **2010**, *9*, 965–974.
(7) Philip, J.; Punnoose, A.; Kim, B. I.; Reddy, K. M.; Layne, S.; Holmes, J. O.; Satpati, B.; Leclair, P. R.; Santos, T. S.; Moodera, J. S. *Nat. Mater.* **2006**, *5* (4), 298–304.
(8) Gupta, A.; Cao, H. T.; Parekh, K.; Rao, K. V.; Raju, A. R.; Waghmare, U. V. *J. Appl. Phys.* **2007**, *101* (9), 09N513–09N513−3.
(9) Kharel, P.; Sudakar, C.; Sahana, M. B.; Lawes, G.; Suryanarayanan, R.; Naik, R.; Naik, V. M. *J. Appl. Phys.* **2007**, *101* (9), 09H117–09H117−3.
(10) Ukah, N. B.; Gupta, R. K.; Kahol, P. K.; Ghosh, K. *Appl. Surf. Sci.* **2009**, *255*, 9420–9424.
(11) Jiang, F. X.; Xu, X. H.; Zhang, J.; Fan, X. C.; Wu, H. S.; Gehring, G. A. *Appl. Phys. Lett.* **2010**, *96* (5), 052503–052503−3.
(12) Ohno, H. *Nat. Mater.* **2010**, *9*, 952–954.
(13) Bizo, L.; Allix, M.; Niu, H.; Rosseinsky, M. J. *Adv. Funct. Mater.* **2008**, *18*, 777–784.
(14) Raebiger, H.; Lany, S.; Zunger, A. *Phys. Rev. Lett.* **2008**, *101*, 027203–027206.
(15) Bourlange, A.; Payne, D. J.; Egdell, R. G.; Foord, J. S.; Edwards, P. P.; Jones, M. O.; Dobson, P. J.; Hutchison, J. L. *Appl. Phys. Lett.* **2008**, *92*, 0921171–09211713.
(16) Walsh, A.; De Silva, J. L. F.; Wei, S.-H.; Korber, C.; Klein, A.; Piper, L. F. J.; DeMasi, A.; Smith, K. E.; Panaccione, G.; Torelli, P.; Payne, D. J.; Bourlange, A.; Egdell, R. G. *Phys. Rev. Lett.* **2008**, *100*, 1674021–1674024.
(17) Huang, L. M.; Silvearv, F.; Araujo, C. M.; Ahuja, R. *Solid State Commun.* **2010**, *150* (13−14), 663–665.
(18) Ogale, S. B. *Adv. Mater.* **2010**, *22*, 3125–3155.
(19) Marquis, E. A.; Miller, M. K.; Blavette, D.; Ringer, S. P.; Sudbrack, C. K.; Smith, G. D. W. *MRS Bull.* **2009**, *34* (10), 725–730.
(20) Marquis, E. A.; Yahya, N. A.; Larson, D. J.; Miller, M. K.; Todd, R. I. *Mater. Today* **2010**, *13* (10), 34–36.
(21) Chen, Y. M.; Ohkubo, T.; Kodzuka, M.; Morita, K.; Hono, K. *Scr. Mater.* **2009**, *61* (7), 693–696.
(22) Larde, R.; Talbot, E.; Vurpillot, F.; Pareige, P.; Schmerber, G.; Beaurepaire, E.; Dinia, A.; Pierron-Bohnes, V. *J. Appl. Phys.* **2009**, *105* (12), 126107–126107−3.
(23) Thompson, K.; Lawrence, D.; Larson, D. J.; Olson, J. D.; Kelly, T. F.; Gorman, B. *Ultramicroscopy* **2007**, *107* (2−3), 131–139.
(24) Bunton, J. H.; Olson, J. D.; Lenz, D. R.; Kelly, T. F. *Microsc. Microanal.* **2007**, *13*, 418–427.
(25) Hellman, O. C.; Vandenbroucke, J. A.; Rüsing, J.; Isheim, D.; Seidman, D. N. *Microsc. Microanal.* **2000**, *6*, 437–444.
(26) Bérardan, D.; Guilmeau, E.; Pelloquin, D. *J. Magn. Magn. Mater.* **2008**, *320*, 983–989.
(27) King, P. D. C.; Veal, T. D.; Fuchs, F.; Wang, C. Y.; Payne, D. J.; Bourlange, A.; Zhang, H. L.; Bell, G. R.; Cimalla, V.; Ambacher, O.; Egdell, R. G.; Bechstedt, F.; McConville, C. F. *Phys. Rev. B* **2009**, *79*, 2052111–205211−10.
(28) King, P. D. C.; Veal, T. D.; Payne, D. J.; Bourlange, A.; Egdell, R. G.; McConville, C. F. *Phys. Rev. Lett.* **2008**, *101*, 116808–116808-4.